Supporting Information

Efficient and Green Synthesis of SiOC Nanoparticles at Near-ambient Condition by Liquid Phase Plasma

Zhiqiang Chen [a, *], Jieming Wang [a], Iuliia Onyshchenko [b], Yichao Wang [a], Christophe Leys [b], Anton Nikiforov [b, *], and Weiwei Lei [a, *]

[a] Institute for Frontier Materials, Deakin University, Waurn Ponds, VIC 3216, Australia

[b] Department of Applied Physics, Ghent University, Sint-Pietersnieuwstraat 41, 9000, Ghent, Belgium

[*]Corresponding authors. zhiqiang.chen@deakin.edu.au (Z.Chen), anton.nikiforov@UGent.be (A. Nikiforov) and weiwei.lei@deakin.edu.au (W. Lei)

KEYWORDS: *green synthesis, liquid phase plasma, optical emission spectroscopy, SiOC nanoparticles*

Number of Pages: 12

Number of Figures :10

Number of Tables: 2

Contents of Supporting Information

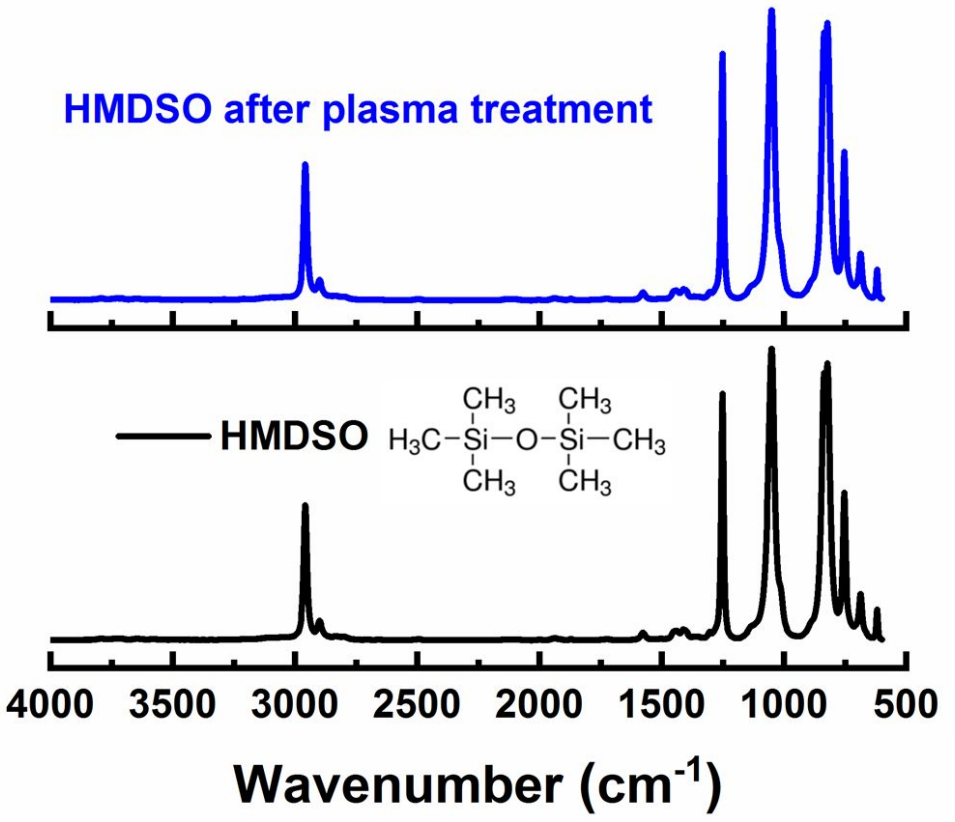

Figure S1. FTIR spectra for HMDSO before and after plasma treatment.

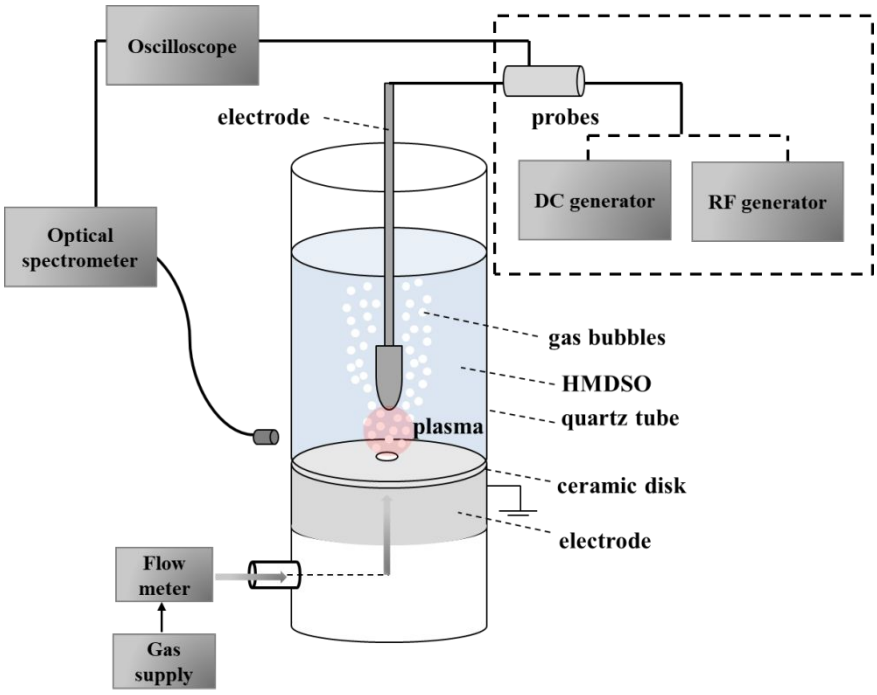

Figure S2. Schematic of the reactor used for NPs production and plasma diagnostics.

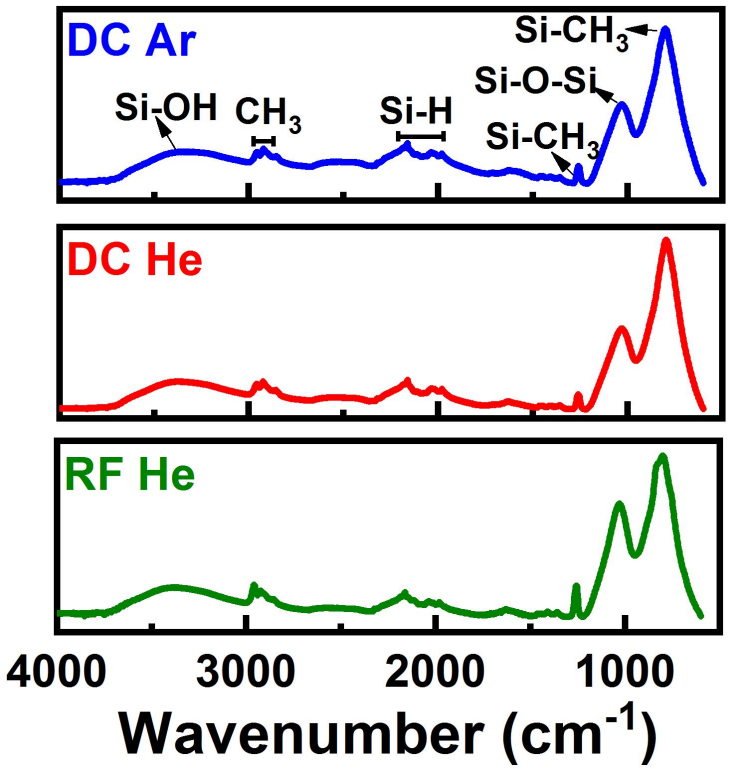

Figure S3. FTIR spectra of SiOC NPs generated in different plasma conditions. For all the DC plasmas, the applied voltages and the distance between electrodes were kept at 9.2 kV and 3mm, respectively; For RF He plasma, the applied power and the distance between electrodes were kept at 90 W and 3mm, respectively.

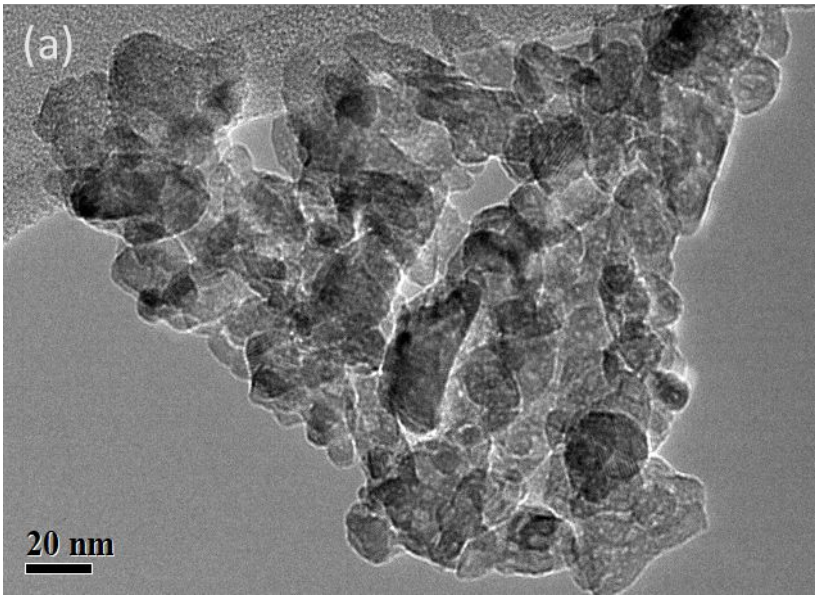

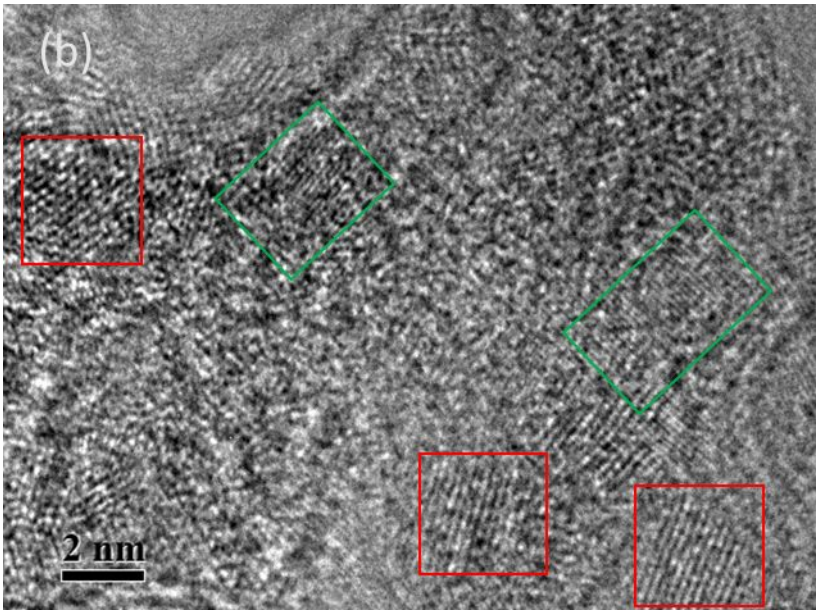
(b)
2 nm

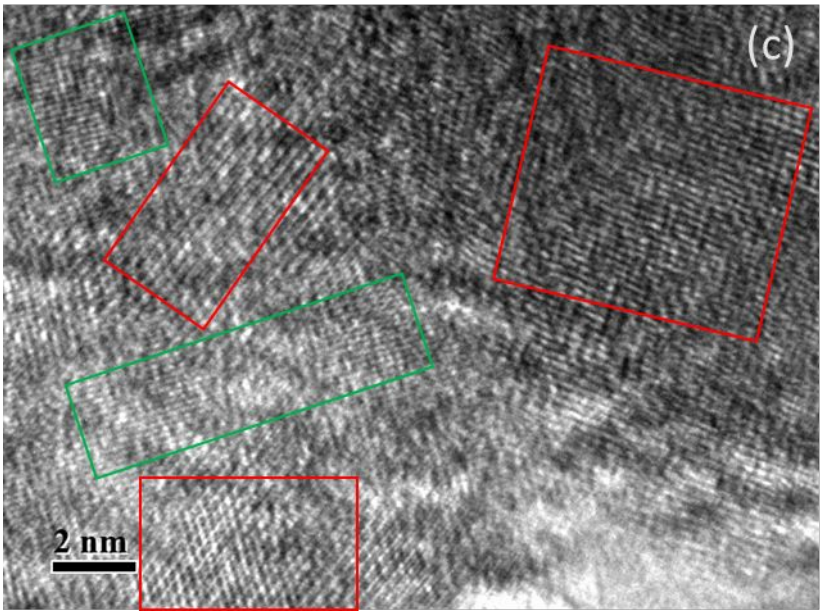
(c)
2 nm

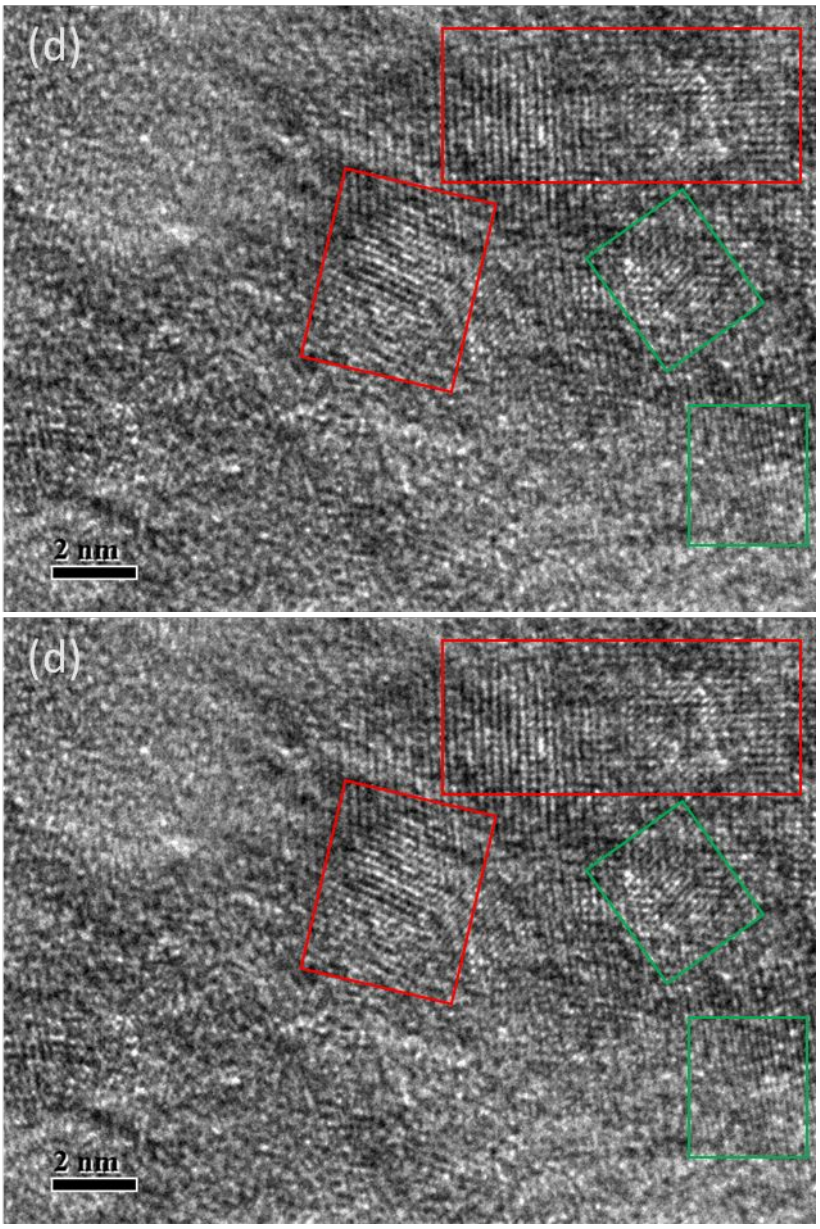
(d)
2 nm
(d)
2 nm

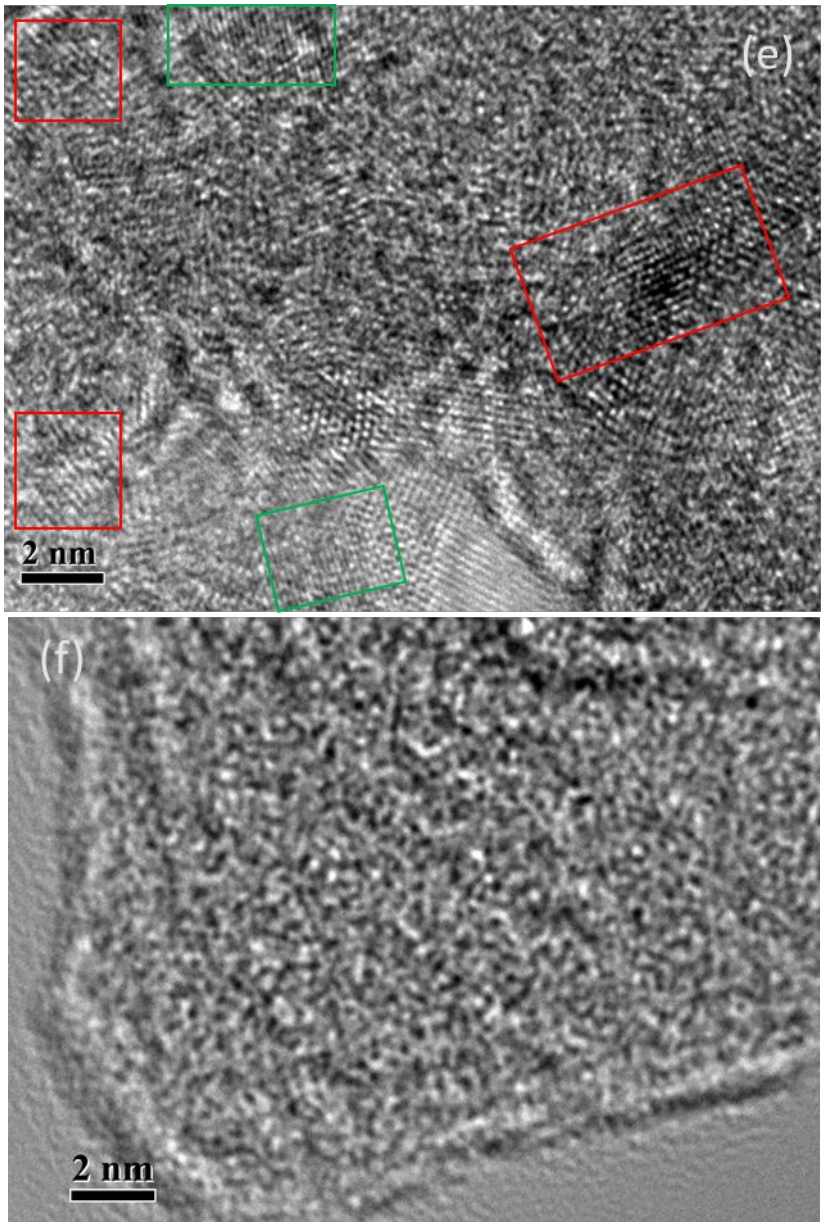

Figure S4. Representative TEM images of as-grown SiOC NPs synthesized by different plasmas. DC Ar plasmas:(a, b) 6.1 kV and (c) 12.1 kV; DC He plasmas :(d) 6.1 kV and (e) 12.1 kV; RF He plasma:(f) 120 W. The distance between electrodes were 3 mm. Graphite-like structure indicated by the red rectangles; crystalline SiC phases indicated by the green rectangles.

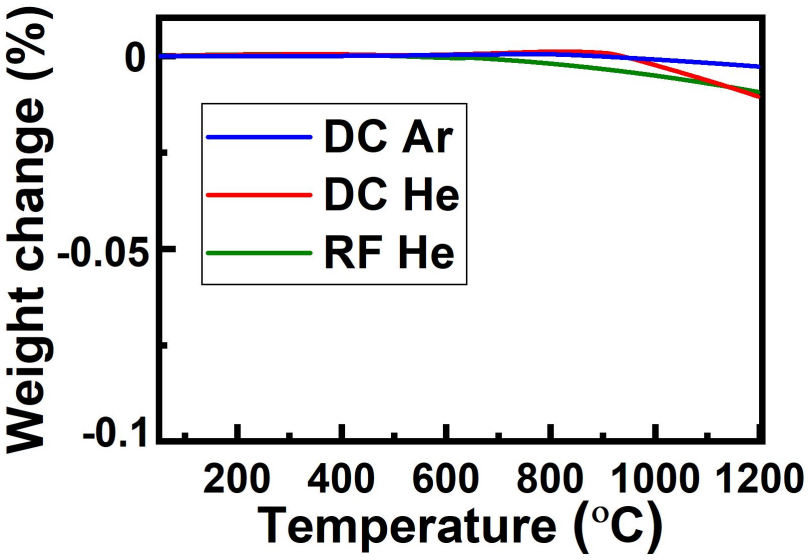

Figure S5. TGA weight change curves for the SiOCs from different plasma conditions.

Table S1. SiOC production rate and energy efficiency under different plasma conditions.

Plasma conditions		Power (W)	Production Of 30s treatment (mg)	Production rate (g/h)	Energy efficiency (g/kWh)
DC Ar, small gap	6.1 kV	76	18.3	2.2	28.9
	9.2 kV	115	40.1	4.8	41.7
	12.1 kV	151	90.2	10.8	71.5
DC He, small gap	6.1 kV	61	9.2	1.1	18.0
	9.2 kV	92	25.8	3.1	33.7
	12.1 kV	121	56.7	6.8	56.2
RF He, small gap		90	9.2	1.1	12.2
		120	16.7	2.0	16.7

Table S2. Atomic concentrations of Si, O and C on the surface of different prepared SiOC samples.

Plasma conditions		Si at. %	O1s at. %	C1s at. %
DC Ar, small gap	6.1 kV	41.7	18.8	39.5
	9.2 kV	42.6	17.8	39.6
	12.1 kV	44.3	16.5	39.2
DC Ar, large gap	6.1 kV	43.3	19.3	37.4
	9.2 kV	41.7	19.2	39.0
	12.1 kV	44.9	17.0	38.1
DC He, small gap	6.1 kV	31.0	28.1	40.9
	9.2 kV	32.0	27.1	40.9
	12.1 kV	30.3	26.0	43.7
DC He, large gap	6.1 kV	33.4	32.7	34.0
	9.2 kV	30.0	27.7	42.3
	12.1 kV	30.2	29.3	40.5
RF He, small gap	70 W	29.5	29.2	41.3
	90 W	30.2	29.1	40.6
	120 W	31.3	29.1	39.7

Plasma Gas Temperature

Two methods were used to determine gas temperature (T_g) based on the OES techniques. First, the presence of the continuum radiation in the DC plasma spectra (Figure 6a) can be used to estimate the gas temperature. In Ar or He discharge, there are several possible sources of continuum radiation. Among them, the excimer radiation appears because of Ar_2^* and He_2^*. The resulting emission is generated in deep UV below 130 nm, which cannot be detected due to the limited sensitivity of the detectors. Another source of the continuum emission is

Bremsstrahlung radiation appearing due to electron-atom and electron-ion interaction.[1] As shown in our previous work,[2, 3] the electron-ion Bremsstrahlung contribution can be neglected due to very low intensity. Moreover, the electron-atom Bremsstrahlung emission should appear in a range around 250-350 nm, depending on electron temperature and electron density. This disagrees with the spectra observed in our experiments. Therefore, the Bremsstrahlung radiation cannot explain the continuum emission visible in Figure 6. The only possible reason for the continuum radiation is the black body radiation, a dominant source of radiation in many thermal plasmas. Therefore, we choose a method from our previous work[4] to estimate gas temperature based on an analysis of the blackbody radiation in accordance with Wien's law:

$$\lambda_{max}[\mathrm{nm}] = \frac{2.89776 \times 10^6\ (\mathrm{nm} \times \mathrm{K})}{T_g(\mathrm{K})} \quad (1)$$

where λ_{max} corresponds to position of blackbody radiation maximum. Moreover, the strong C_2 Swan band was also presented in the optical emission spectra, which offers another method based on the partially resolved rovibrational structure of C_2 Swan band.[5] It should be pointed outpoint out that the rotational temperature of excited states is not always a good indicator of the gas temperature. The rotational temperature can be different from T_g even in conditions of collision dominated plasmas. Our previous work showed that electron impact processes could lead to no thermalization of the rotational states in the case of N_2 plasmas and OH radical emission.[6, 7] The details of this problem have been reviewed in a recent paper.[8] However, it should be noted that in for the C_2 Swan band the rotational-translation transfer results in very fast thermalization of all states. Correspondingly, the C_2 Swan band is one of the cases where rotational temperature can be considered equivalent to T_g.[9-11] For details of the methods and their applicability, we refer the readers to papers.[12, 13] Due to the complexity of the plasma forming process and technical capabilities of optical emission spectroscopy, the emission has been collected from the whole volume of the discharge. It is

challenging to obtain spatially resolved gas temperature measurements inside the bubbles in the plasma/liquid interface. It is worth noting that DC discharge was possible to sustain in Ar, He bubbles in short (3 mm) and long (6 mm) interelectrode gaps whereas RF discharge was only possible to ignite and sustain in He gas bubbles in the short gap of 3 mm.

(1) Iordanova, E.; De Vries, N.; Guillemier, M.; van der Mullen, J. Absolute measurements of the continuum radiation to determine the electron density in a microwave-induced argon plasma. *J. Phys. D: Appl. Phys.* 2007, 41, 015208, DOI: 10.1088/0022-3727/41/1/015208.

(2) Nikiforov, A. Y.; Ionita, E. R.; Dinescu, G.; Leys, C. Characterization of a planar 8 mm atmospheric pressure wide radiofrequency plasma source by spectroscopy techniques. *Plasma Phys. Control. Fusion* 2015, 58, 014013, DOI:10.1088/0741-3335/58/1/014013.

(3) Deng, X; Nikiforov, A. Y.; Ionita, E. R.; Dinescu, G.; Leys, C. Absolute and relative emission spectroscopy study of 3 cm wide planar radio frequency atmospheric pressure bio-plasma source. *Appl. Phys. Lett.* 2015, 107, 053702, DOI: 10.1063/1.4928470.

(4) Vanraes, P.; *Nikiforov, A. Y.*; *Leys*, C. Electrical and spectroscopic characterization of underwater plasma discharge inside rising gas bubbles. *J. Phys. D: Appl. Phys.* 2012, 45, 245206, DOI: 10.1088/0022-3727/45/24/245206.

(5) Elisabeth, C.; Peter De, S.; Anton, Y. N.; Steven, B.; Denis, S.; Werner, B.; Christophe L.; Stefan De, G. Study of ultrasound-assisted radio-frequency plasma discharges in n-dodecane. *J. Phys. D: Appl. Phys*. 2012, 45, 435201, DOI: 10.1088/0022-3727/45/43/435201.

(6) Sremački, I.; Gromov, M.; Leys, C.; Morent, R.; Snyders. R.; Nikiforov, A. An atmospheric pressure non-self-sustained glow discharge in between metal/metal and metal/liquid electrodes. *Plasma Process. Polym*. 2020, 17, e1900191, DOI: 10.1002/ppap.201900191.

(7) Nikiforov, A. Y.; Sarani, A.; Leys, C. The influence of water vapor content on electrical and spectral properties of an atmospheric pressure plasma jet. *Plasma Sources Sci. Technol.* 2011, 20, 015014, DOI: 10.1088/0963-0252/20/1/015014.

(8) Bruggeman, P. J.; Sadeghi, N.; Schram, D. C.; Linss, V. Gas temperature determination from rotational lines in non-equilibrium plasmas: a review. *Plasma Sources Sci. Technol.* 2014, 23, 023001, DOI: 10.1088/0963-0252/23/2/023001.

(9) Lombardi, G.; Bénédic, F.; Mohasseb, F.; Hassouni, K.; Gicquel, A. Determination of gas temperature and C_2 absolute density in $Ar/H_2/CH_4$ microwave discharges used for nanocrystalline diamond deposition from the C_2 Mulliken system. *Plasma Sources Sci. Technol.* 2004,13, 375-386, DOI: 10.1088/0963-0252/13/3/003.

(10) Pellerin, S.; Musiol, K.; Motret, O.; Pokrzywka, B.; Chapelle, J. Application of the (0,0) Swan band spectrum for temperature measurements. *J. Phys. D: Appl. Phys*. 1996, 29, 2850-2865, DOI: 10.1063/1.1614431.

(11) Saito, K.; Sakka, T.; Ogata, Y.H. Rotational spectra and temperature evaluation of C_2 molecules produced by pulsed laser irradiation to a graphite-water interface. *J. Appl. Phys.* 2003, 94, 5530-5536.

(12) Bruggeman, P.; Verreycken, T.; González, M. Á.; Walsh, J. L.; Kong, M. G.; Leys, C.; Schram, D. C. Optical emission spectroscopy as a diagnostic for plasmas in liquids: opportunities and pitfalls. *J. Phys. D: Appl. Phys.* 2010, 43, 124005, DOI: 10.1088/0022-3727/43/12/124005.

(13) Bruggeman, P.; Liu, J.; Degroote, J.; Kong, M. G.; Vierendeels, J.; Leys, C. Dc excited glow discharges in atmospheric pressure air in pin-to-water electrode systems. *J. Phys. D: Appl. Phys.* 2008, 41, 215201, DOI: 10.1088/0022-3727/41/21/215201.